

SELECTED TOPICS IN APPLIED PHYSICS

Characterization of electronic states at insulator/(Al)GaN interfaces for improved insulated gate and surface passivation structures of GaN-based transistors

To cite this article: Zenji Yatabe *et al* 2014 *Jpn. J. Appl. Phys.* **53** 100213

View the [article online](#) for updates and enhancements.

You may also like

- [Engineering of electric field distribution in GaN\(cap\)/AlGaN/GaN heterostructures: theoretical and experimental studies](#)
M Gladysiewicz, L Janicki, J Misiewicz *et al.*
- [Effect of interface and bulk traps on the C–V characterization of a LPCVD-SiN₂/AlGaN/GaN metal-insulator-semiconductor structure](#)
Qilong Bao, Sen Huang, Xinhua Wang *et al.*
- [GaN-based power high-electron-mobility transistors on Si substrates: from materials to devices](#)
Nengtao Wu, Zhiheng Xing, Shanjie Li *et al.*

Characterization of electronic states at insulator/(Al)GaN interfaces for improved insulated gate and surface passivation structures of GaN-based transistors

Zenji Yatabe^{1,2}, Yujin Hori¹, Wan-Cheng Ma¹, Joel T. Asubar^{1,2}, Masamichi Akazawa¹, Taketomo Sato¹, and Tamotsu Hashizume^{1,2*}

¹Graduate School of Information and Science Technology and Research Center for Integrated Quantum Electronics (RCIQE), Hokkaido University, Sapporo 060-8628, Japan

²Japan Science and Technology Agency (JST), CREST, Chiyoda, Tokyo 102-0075, Japan
E-mail: hashi@rciqe.hokudai.ac.jp

Received May 14, 2014; accepted July 8, 2014; published online September 5, 2014

This paper presents a systematic characterization of electronic states at insulators/(Al)GaN interfaces, particularly focusing on insulator/AlGaN/GaN structures. First, we review important results reported for GaN metal–insulator–semiconductor (MIS) structures. SiO₂ is an attractive material for MIS transistor applications due to its large bandgap and high chemical stability. In-situ SiN_x is effective for improving the operation stability of high electron mobility transistors (HEMTs). Meanwhile, Al₂O₃/GaN structures have high band offsets and low interface state densities, which are also desirable for insulated gate applications. We have proposed a calculation method for describing capacitance–voltage (*C*–*V*) characteristics of HEMT MIS structures for evaluating electronic state properties at the insulator/AlGaN interfaces. To evaluate near-midgap states at insulator/AlGaN interfaces, a photo-assisted *C*–*V* technique using photon energies less than the bandgap of GaN has been developed. Using the calculation in conjunction with the photo-assisted *C*–*V* technique, we estimate interface state density distributions at the Al₂O₃/AlGaN interfaces.
© 2014 The Japan Society of Applied Physics

1. Introduction

Advanced GaN-based device technologies have very recently attained a cutoff frequency of 450 GHz and a maximum oscillation frequency of 500 GHz.¹⁾ In addition, excellent power-switching performances with high-blocking voltages and low on-state resistances have been reported for AlGaN/GaN high electron mobility transistors (HEMTs).^{2–7)} Continuous demand for improved device technology has made insulated-gate and surface-passivation structures inevitable for power switching transistors. In particular, the insulating gate dielectric plays an important role in blocking the leakage current when the gate is driven with a forward bias. Furthermore, the deposition of insulator films on the access region surface of the transistor controls surface traps, leading to operation stability and reliability improvement.

In this regard, different insulator materials have been applied to GaN-based transistors including HEMTs. Nonetheless, interface properties of insulator/(Al)GaN structures are still not fully understood. From the viewpoint of the HEMT application, it is desirable to evaluate interface state properties using an actual AlGaN/GaN structure with a very thin AlGaN layer (15–25 nm). However, in comparison with a conventional metal–insulator–semiconductor (MIS) structure having a single semiconductor layer, it is difficult to characterize the insulator/AlGaN interfaces in MIS HEMTs. MIS HEMTs have two interfaces: insulator/AlGaN and AlGaN/GaN, making the potential modulation rather complicated. In addition, the emission efficiency of electrons from the wide-gap interface states to the conduction band is very limited at room temperature (RT).

Although there have been many reports of low interface-trap densities in HEMT MIS capacitors, several papers have incorrectly evaluated their capacitance–voltage (*C*–*V*) characteristics, underestimating the actual interface state density for wide-bandgap semiconductors. When the gate voltage sweeping is confined within the reverse bias region, the resulting *C*–*V* curve often gives rise to misleadingly low density of electronic states at the insulator/AlGaN inter-

faces.^{8,9)} A HEMT MIS structure typically shows a two-step *C*–*V* behavior.¹⁰⁾ However, several groups reported *C*–*V* curves without the characteristic step at the forward bias regime.^{11,12)} In this case, it is likely that high-density states at the insulator/AlGaN interface impede the potential control of the AlGaN surface by the gate bias. In addition, the present GaN-based MIS HEMTs are suffering from threshold voltage fluctuations,^{13–15)} probably due to different charging states of interface traps under different operating conditions. To aid the advancement of insulated gate and surface passivation technologies, suitable characterization methods are needed for understanding the effects of interface states on the *C*–*V* behavior of the HEMT MIS structures. A combination of recessed and insulated gates is often used in normally-off AlGaN/GaN HEMTs. Since the interface quality greatly affects the transistor performance, evaluating interface properties of HEMT MIS structures fabricated on the dry-etched AlGaN surfaces is suitably important.

Accordingly, this paper presents characterization of electronic states at insulators/(Al)GaN interfaces, particularly focusing on insulator/AlGaN/GaN structures. First, we review important results reported for GaN-based MIS structures. We have developed a numerical calculation method for obtaining *C*–*V* characteristics of HEMT MIS structures. Using this method, we then present the effects of electronic states at the insulator/AlGaN interface on the *C*–*V* behavior of HEMT MIS capacitors. To evaluate near-midgap interface states at RT, we have proposed a photo-assisted *C*–*V* characterization technique using photon energies less than the bandgap of GaN. On the basis of the calculation and the photo-assisted *C*–*V* analysis, we estimate interface state density distributions at the Al₂O₃/AlGaN interfaces with and without dry etching of the AlGaN surface.

2. Band lineups between GaN and relevant insulator materials

For a structure design of an MIS transistor or a surface-passivated transistor using a wide-gap semiconductor, it is important to understand the band lineup between the

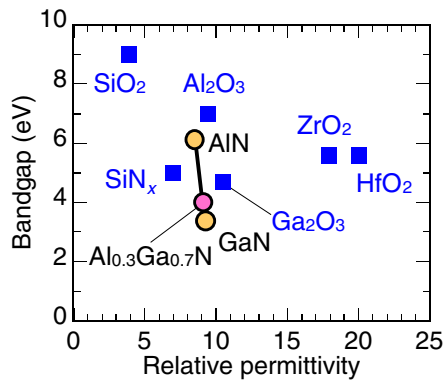


Fig. 1. (Color online) Energy gap E_G versus dielectric constant ϵ for various insulators and GaN compounds.

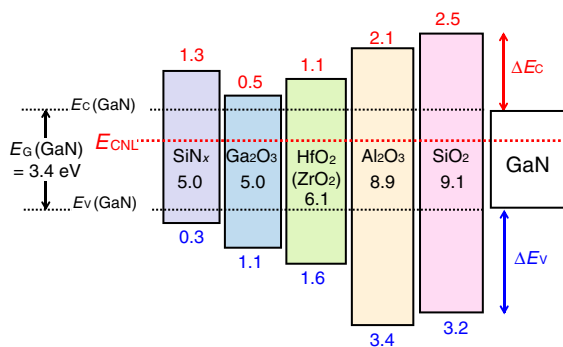


Fig. 2. (Color online) Band lineups at insulators/GaN interfaces calculated by Robertson and Falabretti.¹⁶⁾ The charge neutrality level, E_{CNL} , acts as the reference energy level for the lineup. Note that the bandgap of Al_2O_3 used in the calculation is that of the bulk, which is higher than that of an amorphous film reported experimentally.

insulator and the semiconductor involved. Figure 1 shows the plot of energy gap versus dielectric constant for relevant insulators and nitride compounds. It is a common knowledge that a higher value of dielectric constant leads to a higher value of transconductance g_m . From this point of view, SiO_2 is at a disadvantage compared with the other dielectric materials. Also, a large band-offset energy is required at the insulator/AlGaIn interface for the suppression of leakage current. On this account, MIS gate structures employing Si_3N_4 , ZrO_2 , and HfO_2 dielectric materials are relatively susceptible to leakage current problems. On the other hand, Al_2O_3 is one of the most attractive dielectric materials for power MIS devices because it combines all the desired properties such as large bandgap, relatively high dielectric constant, and high breakdown field (~ 10 MV/cm).

Figure 2 shows the band lineups between GaN and several insulators reported by Robertson and Falabretti.¹⁶⁾ They calculated charge neutrality levels (E_{CNL}) for GaN and insulators and determined the lineup using E_{CNL} as the reference energy level. All interfaces result in the type-I alignment. Note that the bandgap of Al_2O_3 used in the calculation is that of the bulk, which is higher than those values (6.7–7.0 eV) obtained experimentally from amorphous films.^{17–19)} Calculations predict that Ga_2O_3 , SiNx and HfO_2 interfaces produce relatively low barriers at the conduction band ΔE_C . Similar values were obtained from X-ray photoelectron

spectroscopy analyses and leakage current characterizations.^{20–25)} Relatively high leakage current may arise at forward bias when these insulators are used in the insulated gate structures. On the other hand, the resulting ΔE_C values from Al_2O_3 and SiO_2 are high enough for gate applications.^{17,26–28)}

3. Interface properties of GaN MIS structures

3.1 SiO_2/GaN structure

Gaffey et al.²⁶⁾ reported a precise characterization of interface properties of a $\text{SiO}_2/\text{SiNx}/\text{SiO}_2/\text{n-GaN}$ structure prepared by jet vapor deposition. From the conductance–frequency analysis, they obtained a state density of $5 \times 10^{10} \text{ cm}^{-2} \text{ eV}^{-1}$ at $E_C - 0.8 \text{ eV}$ with a capture cross section of $2.4 \times 10^{-17} \text{ cm}^2$ for the MIS sample fabricated using the optimum process condition. Matocha et al.²⁹⁾ and Kim et al.³⁰⁾ presented low state densities at the $\text{SiO}_2/\text{n-GaN}$ interfaces prepared at high temperatures (830–900 °C). Kanechika et al.³¹⁾ fabricated a vertical-type AlGaIn/GaN MOS HEMT, demonstrating good I – V characteristics with a high on/off ratio using a SiO_2 film thermally deposited at 830 °C. It was also found that high-temperature annealing process after the SiO_2 deposition was also effective in decreasing the interface state density.^{32–35)} Kambayashi et al.³⁴⁾ reported over 100 A operation in AlGaIn/GaN hybrid HEMT using the SiO_2 gate dielectric post-deposition annealed at 700 °C. Very recently, a channel mobility of $192 \text{ cm}^2 \text{ V}^{-1} \text{ s}^{-1}$ was achieved in a hybrid HEMT using a $\text{Al}_2\text{O}_3/\text{SiO}_2$ bilayer gate structure.³⁶⁾ Although the SiO_2 film has a low permittivity as shown in Fig. 1, it remains attractive for MIS HEMT applications because of its large bandgap and chemical stability.

3.2 SiNx/GaN structure

The SiNx film is widely used for surface passivation of GaN-based transistors. Hashizume et al.^{20,37)} demonstrated that the SiNx deposition on N_2 -plasma treated surfaces can produce a good $\text{SiNx}/\text{n-GaN}$ interface with a state density as low as $1 \times 10^{11} \text{ cm}^{-2} \text{ eV}^{-1}$ at $E_C - 0.8 \text{ eV}$. The reason for the low interface state densities at the $\text{SiNx}/\text{n-GaN}$ interface is not yet fully understood. It is likely that nitrogen radicals generated during the SiNx deposition process control the formation of nitrogen-vacancy-related defects at the GaN surface,³⁸⁾ leading to the prevention of interface electronic states. Green et al.³⁹⁾ were the first to apply- SiNx passivation to the AlGaIn/GaN HEMTs, and have observed a significant improvement of microwave output power as a consequence.

The in-situ deposition of SiNx is an interesting process in the sense that it can be performed in the same growth chamber and in the same growth sequence as the rest of the layer stack.⁴⁰⁾ During the final growth stage of the AlGaIn/GaN structure by metal organic chemical vapor deposition, the SiNx layer was in-situ deposited using NH_3 and SiH_4 on the AlGaIn surface at 1020 °C. Derluyn et al.⁴⁰⁾ obtained improved I – V characteristics from HEMTs with the in-situ deposited SiNx layer. The in-situ process realized an oxide-free $\text{SiNx}/\text{AlGaIn}$ interface.⁴¹⁾ From the high-resolution transmission electron microscopy (HR-TEM) analysis, Takizawa et al.⁴²⁾ reported that the in-situ SiNx has a single crystalline structure. Very recently, Van Hove et al.³⁾ demonstrated that an AlGaIn/GaN HEMT with a stable threshold

voltage and a low current collapse can be achieved using an in-situ $\text{SiN}_x/\text{Al}_2\text{O}_3$ bilayer gate.

3.3 $\text{Al}_2\text{O}_3/\text{GaN}$ structure

As mentioned in Sect. 2, the Al_2O_3 has a large bandgap, a relatively high dielectric constant and a high breakdown field. In addition, there has been considerable progress of atomic layer deposition (ALD) technology, simplifying the application of Al_2O_3 to the gate and passivation structures in the GaN transistors.^{43–45} Park et al.⁴⁶ were the first to report AlGaIn/GaN MOS HEMTs using an Al_2O_3 prepared by ALD as a gate dielectric and a surface passivation layer. The ALD process realized good $\text{Al}_2\text{O}_3/\text{n-GaN}$ interface with a low state density of around $1 \times 10^{11} \text{ cm}^{-2} \text{ eV}^{-1}$ at $E_C - 0.8 \text{ eV}$.^{17,47}

When using Al_2O_3 , special attention should be given to subsequent process temperatures. From the transmission electron microscope (TEM) observation, Hori et al.¹⁷ found a flat and smooth atomic arrangement around the ALD prepared amorphous $\text{Al}_2\text{O}_3/\text{n-GaN}$ interface. However, annealing at 800°C for the formation of ohmic electrodes generated a large number of microcrystallized regions in the Al_2O_3 layer, causing a marked increase in the leakage current of the $\text{Al}_2\text{O}_3/\text{GaN}$ structure. Toyoda et al.⁴⁸ also reported that annealing procedures at 800°C resulted in the phase transformation of Al_2O_3 films from amorphous to crystalline. To address this issue, an ohmic-first process, i.e., formation of ohmic electrodes including annealing at 800°C before the Al_2O_3 deposition, was developed for $\text{Al}_2\text{O}_3/\text{n-GaN}$ structures.¹⁷ This method effectively suppresses leakage current in MOS structures. Nevertheless, even in this scheme, a surface protection layer is indispensable to avoid the chemical bond disorder at the GaN surface during the annealing process. Optimization of the ohmic-first process using a SiN_x surface protection layer then realized a good $\text{Al}_2\text{O}_3/\text{n-GaN}$ interface with a low state density of $2 \times 10^{11} \text{ cm}^{-2} \text{ eV}^{-1}$ at $E_C - 0.8 \text{ eV}$.¹⁷

For practical applications of Al_2O_3 to the MOS HEMTs, stability and reliability characterization of the Al_2O_3 films is necessary. From a time-dependent dielectric breakdown measurement, Kikuta et al.⁴⁹ reported that a time-to-breakdown (t_{BD}) at 3 MV/cm for the ALD- Al_2O_3 film was more than 40000 years at RT. However, the t_{BD} significantly decreased to 10^2 – 10^3 s at 250°C . Esposto et al.²⁸ and Son et al.⁵⁰ pointed out that relatively high densities of fixed charges in Al_2O_3 films shifted flat-band voltages in the C – V curves of the $\text{Al}_2\text{O}_3/\text{n-GaN}$ capacitors. The origin for the fixed charges is not clear yet. Choi et al.⁵¹ theoretically predicted that the oxygen vacancy in Al_2O_3 introduces transition levels close to the conduction band edge of GaN, and it can act as border traps at the $\text{Al}_2\text{O}_3/\text{n-GaN}$ interface. On the other hand, it is likely that other kinds of defects such as Al vacancy and interstitials act as fixed charges in Al_2O_3 .⁵¹

3.4 High- κ insulators/GaN structure

High- κ insulators are attractive for the MIS transistors for achieving high g_m . Recently, relatively good I – V characteristics were reported for AlGaIn/GaN HEMTs with high- κ gate insulators.^{52–55} Hatano et al.⁵⁵ demonstrated the improved operation stability in the AlGaIn/GaN HEMT with

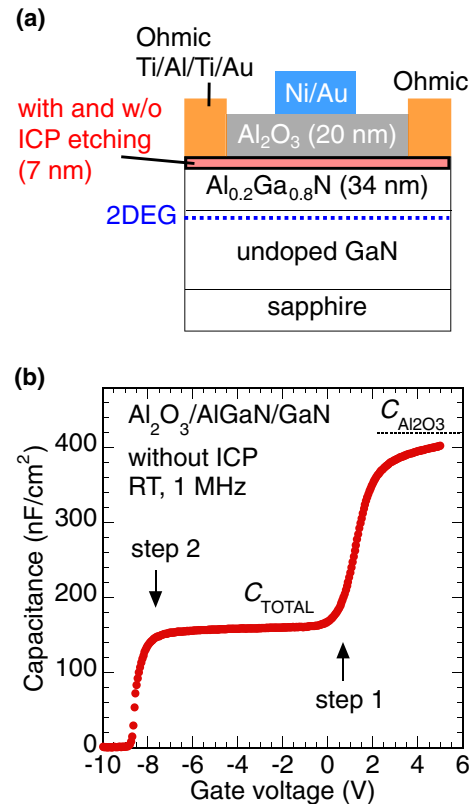


Fig. 3. (Color online) (a) Schematic illustration of the $\text{Al}_2\text{O}_3/\text{AlGaIn}/\text{GaN}$ structure and (b) RT C – V curve of the HEMT MOS sample without ICP etching of AlGaIn.

an $\text{Al}_2\text{O}_3/\text{ZrO}_2$ bilayer gate dielectric. However, interface properties of high- κ/AlGaIn structures are not well understood. In addition, severe V_{th} fluctuations were reported by Hayashi et al.⁵⁶ and Stoklas et al.⁵⁷ in HEMTs with HfO_2 - and ZrO_2 -gate dielectric materials, respectively. Therefore, further investigation is necessary to gain better understanding of high- κ insulators/(Al)GaN interfaces.

4. HEMT MIS structures

4.1 Interpretation of HEMT MIS C – V characteristics

To improve device performance and stability of MIS HEMTs using AlGaIn/GaN and InAlN/GaN structures, evaluation of electronic state properties of the interfaces between insulators and AlGaIn/InAlN is of utmost importance. However, fabrication of a simple MIS diode using a thick AlGaIn or InAlN is challenging due to the difficulty of growing high-quality epitaxial layers. For the practical device application, it is desirable to characterize insulator/AlGaIn or insulator/InAlN interfaces using HEMT MIS structures. In this regard, we initially attempt to interpret precisely the resulting C – V characteristics of the HEMT MIS structures.

Figure 3(a) shows a schematic illustration of the HEMT MIS structure used in this study. An undoped AlGaIn/GaN heterostructure grown on a sapphire substrate by metal organic chemical vapor deposition (MOCVD) was used as the starting wafer (provided by NTT-AT). The sheet resistance and mobility of the AlGaIn/GaN heterostructure were $500 \Omega/\text{sq.}$ and $1750 \text{ cm}^2 \text{ V}^{-1} \text{ s}^{-1}$, respectively. We prepared $\text{Al}_2\text{O}_3/\text{AlGaIn}/\text{GaN}$ samples with and without dry etching

Table I. Parameters used in the calculations. Φ_B is the Schottky barrier height at the metal/insulator interface. ΔE_{C1} and ΔE_{C2} are the conduction-band offsets between insulator/AlGaIn and AlGaIn/GaN interfaces, respectively (Ref. 16).

	SiO ₂	SiN _x	Al ₂ O ₃	HfO ₂
E_G (eV)	8.9	4.9	6.7	5.6
ϵ_r	3.9	7.0	9.0	15
Φ_B (eV)	3.7	3.1	3.5	3.2
ΔE_{C1} (eV)	2.5	1.3	2.1	1.1
ΔE_{C2} (eV)	0.3	0.3	0.3	0.3

of the AlGaIn surface. For the etching of AlGaIn, we used a Cl₂-based dry etching process assisted by inductively coupled plasma (ICP) at RT. The ICP and bias powers were 300 and 5 W, respectively. The resulting etching depth was 7 nm. We then deposited a 10-nm-thick SiN_x film as a surface protection layer to avoid damage to the AlGaIn surface during ohmic annealing.¹⁷⁾ As an ohmic electrode, a ring-shaped Ti/Al/Ti/Au multilayer structure was deposited on the AlGaIn surface, followed by annealing at 800 °C for 1 min in N₂ ambient. After removing the SiN_x film, an Al₂O₃ layer with a nominal thickness of 20 nm was deposited at a deposition rate of 0.11 nm/cycle on the AlGaIn surface using an ALD system (SUGA-SAL1500) at 350 °C for 170 cycles. During the deposition process, water vapor and TMA were introduced into an ALD reactor in alternate pulse forms. Finally, a circular Ni/Au (20/50 nm) gate electrode concentric with the ohmic electrode was deposited on the Al₂O₃ layer.

Figure 3(b) shows a typical C - V curve of the Al₂O₃/AlGaIn/GaN structure without the etching of the AlGaIn surface. C - V measurements were carried out using an impedance analyzer (HP4192 LF) with a measurement frequency of 1 MHz at RT. A characteristic C - V curve with two steps was observed, which is peculiar to the MIS structure fabricated on the heterostructure including a two-dimensional electron gas (2DEG).^{10,44,58,59)} The constant capacitance at the forward bias corresponds to the Al₂O₃ capacitance, whereas that at the reverse bias is determined by the total capacitance (C_{TOTAL}) of the Al₂O₃ and AlGaIn layers. At a deep reverse bias, the capacitance steeply decreases to nearly zero, indicating the 2DEG depletion at the AlGaIn/GaN interface.

To understand this peculiar C - V behavior, we carried out calculations using a numerical solver of the Poisson equation based on the one-dimensional Gummel algorithm, taking into account the fixed charge at the AlGaIn/GaN interface originating from spontaneous and piezoelectric polarization as well as the charge in the electronic states at the insulator/AlGaIn interface.⁶⁰⁾ We assumed the 2DEG density of $1 \times 10^{13} \text{ cm}^{-2}$ and an insulator thickness of 20 nm. Other parameters used in calculation are listed in Table I, where Φ_B is the Schottky barrier height at the metal/insulator interface, ΔE_{C1} and ΔE_{C2} are the conduction-band offsets between insulator/AlGaIn and AlGaIn/GaN interfaces, respectively. Figure 4(a) shows the calculated MIS C - V curves neglecting interface state density (ideal curve) for various insulators. The two-step behavior is reproduced in all HEMT MIS structures. Insulator capacitance, total capacitance (C_{TOTAL}) and threshold voltage

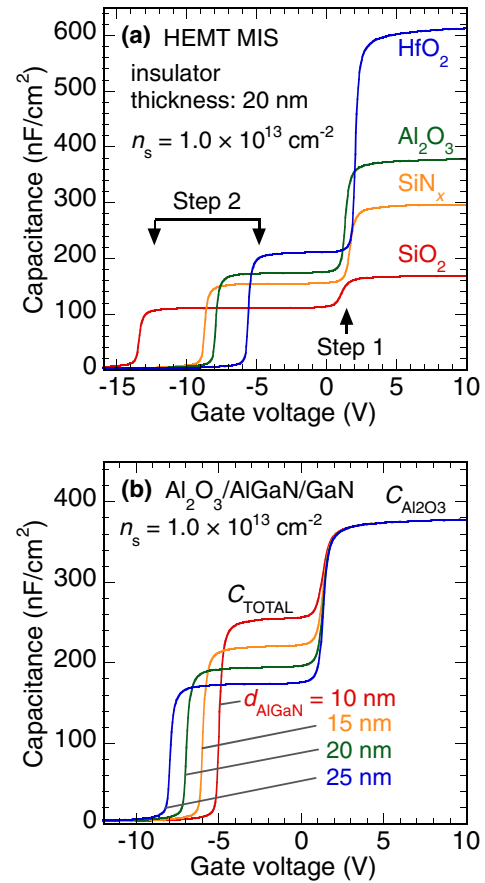


Fig. 4. (Color online) (a) The calculated C - V curves of HEMT MIS structures using some insulators without considering interface state density (ideal curve). (b) AlGaIn-thickness dependence of C - V curves for the Al₂O₃/AlGaIn/GaN structure.

at the step 2 systematically change along with the changing value of permittivity as expected. The AlGaIn-thickness dependence of the C - V curves is shown in Fig. 4(b). Similarly, a systematic change is seen in C_{TOTAL} and the threshold voltage.

The ideal curves show almost the same slope at both steps 1 and 2. This is completely different from the experimental result shown in Fig. 3(b). To shed a light on this, we carried out calculations for the Al₂O₃/AlGaIn/GaN structure, taking into account the effect of interface electronic states.⁶⁰⁾ Figure 5(a) shows the interface state density distributions $D_{it}(E)$ used in calculation, illustrating the acceptor- and donor-like states divided by the charge neutrality level E_{CNL} .^{60,61)} We adapted the E_{CNL} values calculated by Mönch in Ref. 62. In addition, we used electron emission time constant τ from interface states to the conduction band calculated using Shockley-Read-Hall (SRH) statistics:

$$\tau = \frac{1}{v_{\text{TH}} \sigma_{\text{TH}} N_{\text{C}}} \exp\left(\frac{E_{\text{T}}}{kT}\right), \quad (1)$$

where v_{TH} , σ_{TH} , N_{C} , and E_{T} are electron thermal velocity, capture cross section, density of state at the conduction band, and interface state energy, respectively.

The calculated C - V curves are shown in Fig. 5(b). In the forward bias region, the C - V slope drastically decreases with increasing interface state density, similar to the experimental results. At forward bias, the nearly flat potential of the AlGaIn

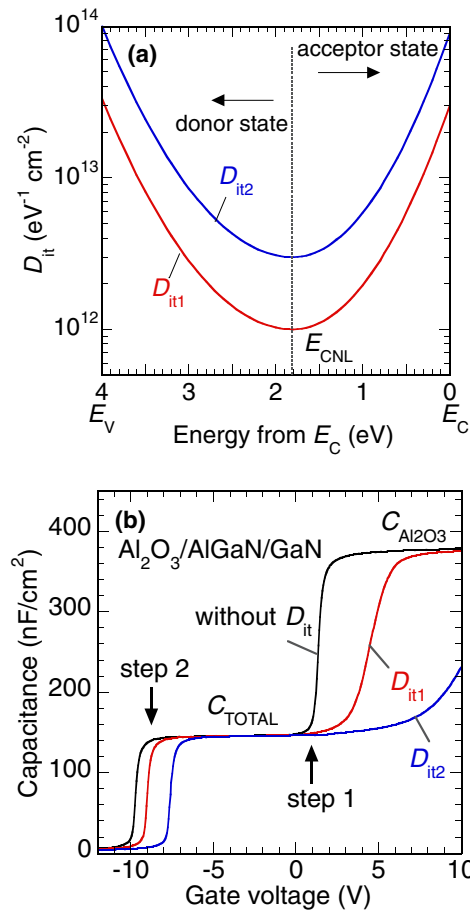


Fig. 5. (Color online) (a) Interface density distributions used in calculation and (b) the calculated C - V characteristics of the $\text{Al}_2\text{O}_3/\text{AlGaIn}/\text{GaIn}$ structure with and without considering interface states.

layer shown in Fig. 6(a) can lead to the electron transfer with ease from the $\text{AlGaIn}/\text{GaIn}$ interface to the $\text{Al}_2\text{O}_3/\text{AlGaIn}$ interface, resulting in the steep C - V slope relative to the case without interface states. However, in the actual case, electron trapping at the $\text{Al}_2\text{O}_3/\text{AlGaIn}$ interface states is highly probable. The acceptor-type states result in excess negative charges when they trap electrons. Such negatively charged interface states can screen the gate electric field, suppressing the potential modulation of the AlGaIn layer. This causes the stretch out of the C - V curve, as shown in Fig. 5(b). In an extreme case, if a HEMT MIS sample includes very high interface state densities, then the step 1 will not be observed even at high forward bias. Indeed, several papers showed no C - V step even at high forward bias.^{11,12} On the other hand, in the reverse bias region, the stretch-out behavior was not observed in the C - V curve. Figure 6(b) shows the potential distribution at $V_G = -8$ V. The Fermi level (E_F) is located far below the valence band maximum of AlGaIn at the $\text{Al}_2\text{O}_3/\text{AlGaIn}$ interface, which makes electron occupation of interface states no longer a function of the gate bias, leading to absence of stretch-out behavior in the C - V curve. In addition, Eq. (1) gives very long time constants of electron emission from deep states to conduction band. Therefore, electrons captured at deep states remain unaffected even when a large negative bias is applied to the gate electrode. This leads to the fact that the interface states act as “fixed and frozen” charges.

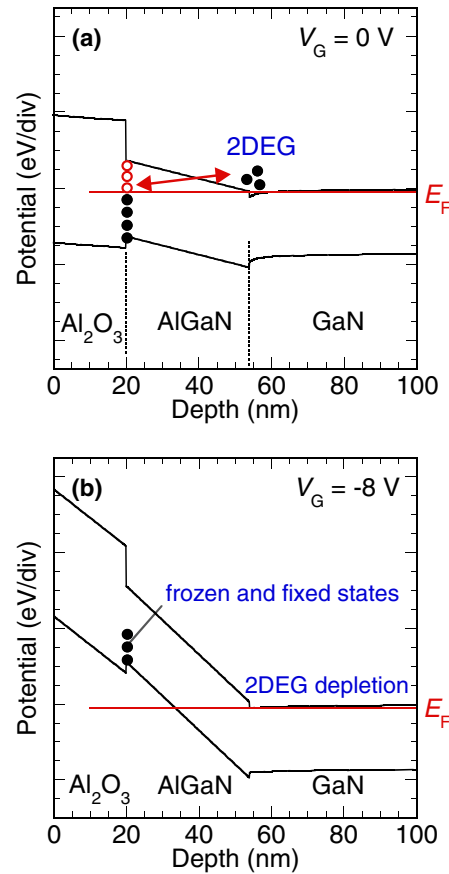


Fig. 6. (Color online) Band diagrams of the $\text{Al}_2\text{O}_3/\text{AlGaIn}/\text{GaIn}$ structure at (a) $V_G = 0$ and (b) $V_G = -8$ V.

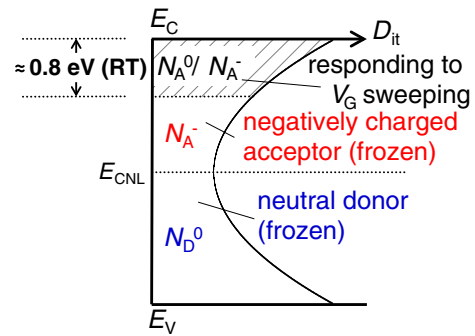


Fig. 7. (Color online) Schematic illustration of charge condition of the interface states at RT. N_A^0 and N_D^0 indicate the neutral acceptor and donor states, respectively, and N_A^- denotes the negatively charged acceptor state.

Figure 7 schematically shows the charge condition of the interface states at RT. When a value of $1 \times 10^{-16} \text{ cm}^2$ is used for the capture cross section of the interface states, only the upper half of the acceptor-like traps can change their charge state (N_A^0/N_A^-) accordingly with the gate voltage sweep. The acceptor-type states in this energy region produce excess negative charges when electrons are trapped, whereas they are in the neutral charge state when electrons are detrapped, mainly causing the stretch out of the C - V curve at the forward bias. Due to the associated long emission time constants, electrons in the lower half of acceptor-like traps remain trapped and act as negatively fixed charges, even

when the E_F is located far below the valence band maximum of AlGaIn [Fig. 6(b)]. This leads to the parallel C - V shift (V_{th} shift) at step 2 toward the positive bias direction with respect to the ideal C - V curve, as shown in Fig. 5(b). The V_{th} shift is enhanced with increasing interface state density. Similarly, the donor-like traps remain on their neutral charge state (filled with electrons), independent of the bias sweeping. Since their neutral condition remains unchanged at RT, it is rather difficult to evaluate the effect of the donor-like traps by a standard C - V measurement.

The conductance method is often applied in HEMT MIS structures to analyze interface states.^{63–65} Using this technique, careful attention should be given to the E_F position at the insulator/AlGaIn interface. At reverse bias regime, the interface states could not be responsible for the conductance peak in the conductance–frequency (G - f) curve,^{63,64} because of the associated long emission time constants of interface states. In addition, Shih et al.⁶⁵ pointed out that the conventional conductance method is viable only for a narrow range of gate bias voltages, and invalid for the analysis of deeper interface states. They proposed a unique characterization method using G - f characteristics at forward bias and high temperatures. From an analysis based on the G - f - T (temperature) mapping, they estimated an energy range of interface states responding to the G - f measurement and a gate control efficiency related to an interface state density.⁶⁵

4.2 Photo-assisted C - V analysis

To evaluate near-midgap electronic states at insulator/AlGaIn interfaces at RT, we have developed a photo-assisted C - V method.¹⁰ Figure 8 shows schematic illustrations of photo-ionization effects of interface states under a monochromatic light with energy less than the bandgap of GaN. First, under dark condition, a forward gate voltage high enough to observe the insulator capacitance is applied. At this state, almost all of interface traps are filled with electrons under a nearly flat band condition. Then, the gate bias is swept toward a value more negative than the threshold voltage. After reaching a sufficiently negative gate bias, a monochromatic light with photon energy of $h\nu_1$ is illuminated to the sample surface. Consequently, we are effectively inducing photo-assisted electron emission from the interface states within the energy range corresponding to the photon energy range, as schematically shown in Fig. 8(a). After switching the light off, we restarted the voltage sweep toward 0 V under dark condition. As shown Fig. 8(b), we can observe the C - V curve shift toward the reverse bias direction, corresponding to the change in the interface state charge Q_{it} ($h\nu_1$).

Using different photon energies, we can induce a systematic C - V shift according to the photon energy, as shown in Fig. 8(b). The voltage shift difference (ΔV) between two photon energies corresponds to the interface charge difference, ΔQ_{it} , in the energy range $\Delta h\nu$ shown in Fig. 8(c). The state density can be simply estimated using the observed ΔV in the following equation:

$$D_{it}(E = E_{AV}) = \frac{C_{TOTAL} \cdot \Delta V}{q \cdot \Delta h\nu}, \quad (2)$$

where C_{TOTAL} is the total capacitance of Al₂O₃ and AlGaIn and E_{AV} is the average interface energy schematically shown in Fig. 8(c).

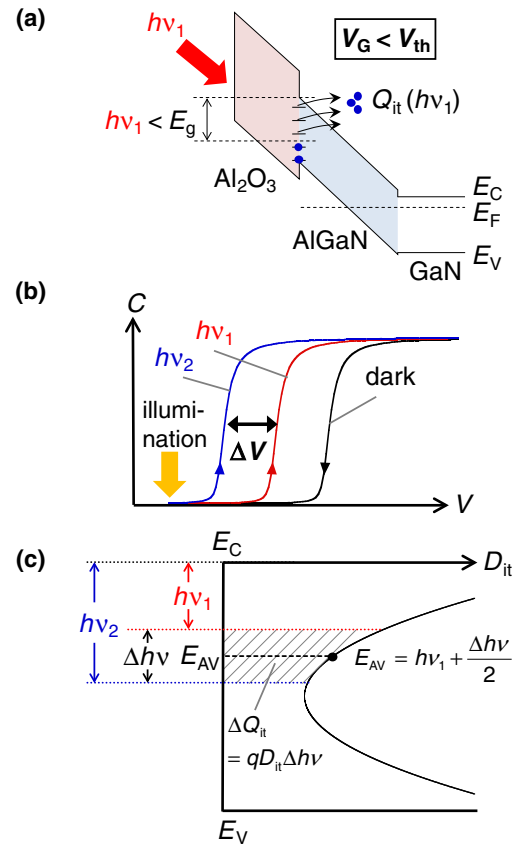


Fig. 8. (Color online) Schematic illustration of (a) photo-assisted electron emission at the Al₂O₃/AlGaIn interface, (b) photo-assisted C - V characteristics and (c) interface state charge and energy range corresponding to the voltage shift, ΔV , in photo-assisted C - V curves.

It should be emphasized that the present method uses incident photons with energies less than the bandgap of GaN. On the other hand, some groups have reported photo-assisted C - V characterization of MIS structures using a light source with photon energies larger than the GaN bandgap.^{66,67} In this case, holes are generated and accumulated at insulator/AlGaIn and AlGaIn/GaN interfaces. In addition, interaction of holes with the interface states especially at reverse bias has to be considered. This makes the charge dynamics in HEMT MIS structures complicated and the evaluation of interface state states very difficult. Very recently, Matys et al.^{68,69} proposed a simulation method for the photo-assisted C - V characteristics, taking into account the electron–hole generation and the recombination processes as well as the hole capture process at the interface states. Comparing their calculation results to the experimental data, they were able to estimate the state density distribution at the Al₂O₃/AlGaIn interface near the valence-band maximum of AlGaIn.

4.3 Estimation of the state density distribution at Al₂O₃/AlGaIn interface using HEMT MIS structures

Using the combination of the numerical fitting of C - V curves and the photo-assisted C - V method, we have attempted to estimate the state density distribution of the Al₂O₃/AlGaIn interfaces. Figure 9(a) shows the comparison between the calculated and experimental C - V curves of the Al₂O₃/AlGaIn/GaN structure with and without the ICP dry etching

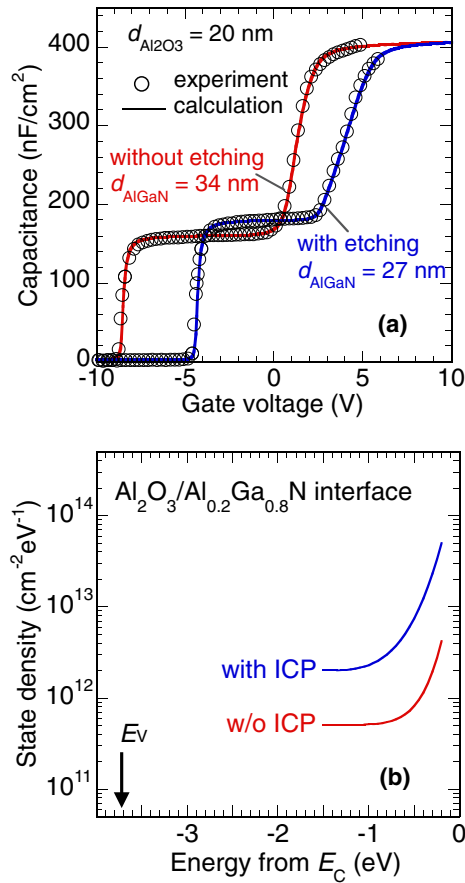


Fig. 9. (Color online) (a) The comparison between the calculated and experimental C - V curves of the $\text{Al}_2\text{O}_3/\text{AlGaIn}/\text{GaN}$ structure with and without the ICP etching of AlGaIn. By assuming interface state density distributions indicated by the solid lines in (b), the calculation reasonably reproduced the experimental data.

of the AlGaIn surface. As shown in Fig. 3(a), the initial HEMT structure has a 34-nm-thick AlGaIn layer. After the ICP etching, the AlGaIn thickness was reduced to 27 nm,⁷⁰ causing an increase in C_{TOTAL} and a pronounced V_{th} shift in the C - V curve. By assuming interface state density distributions indicated by the solid lines in Fig. 9(b), the calculation reasonably reproduced the experimental data. From the fitting results, we can determine the state density distribution near E_c at the $\text{Al}_2\text{O}_3/\text{AlGaIn}$ interface. Note that it is difficult to evaluate the state density distribution at the energies above $E_c - 0.2$ eV from C - V measurements at the frequency of 1 MHz, because electrons captured at such shallow interface states can respond to the measurement AC signal and accordingly give an inaccurate estimate of capacitance.

Figure 10 shows the measured photo-assisted C - V curves of the sample with the ICP etching of AlGaIn. We observed systematic C - V shifts toward the reverse bias direction with increasing photon energy, as explained in Sect. 4.2. The completely parallel C - V shift toward the negative direction indicates that the interface states near midgap or at deeper energies act as fixed charges in this bias range. Ozaki et al.⁷¹ recently reported a similar parallel C - V shift in an ALD- $\text{Al}_2\text{O}_3/\text{n-GaN}/\text{AlGaIn}/\text{GaN}$ structure. Using Eq. (2), we estimated the interface state densities in the samples with and without the ICP etching of AlGaIn. Figure 11 shows

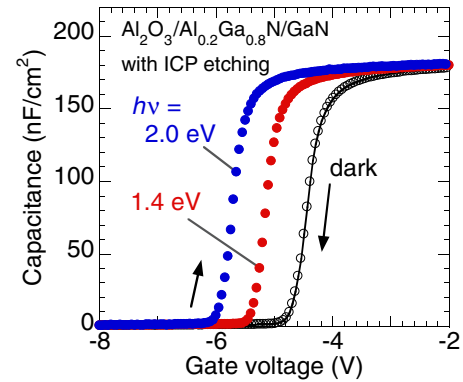


Fig. 10. (Color online) Photo-assisted C - V characteristic of $\text{Al}_2\text{O}_3/\text{AlGaIn}/\text{GaN}$ structure with ICP etching of AlGaIn.

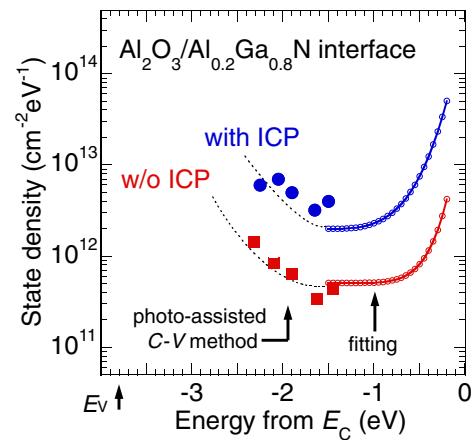


Fig. 11. (Color online) State density distributions at the $\text{Al}_2\text{O}_3/\text{AlGaIn}$ interface determined by a combination of the photo-assisted C - V method and the C - V fitting analysis.

the state density distributions at the $\text{Al}_2\text{O}_3/\text{AlGaIn}$ interface determined by the photo-assisted C - V and the fitting methods. The sample without the ICP etching of AlGaIn showed state densities of around $1 \times 10^{12} \text{ cm}^{-2} \text{ eV}^{-1}$ or less near the midgap. On the other hand, much higher state densities were obtained at the $\text{Al}_2\text{O}_3/\text{ICP-etched AlGaIn}$ interface.

From transmission electron microscopy (TEM) observations, it was found that the ICP etching process introduced a monolayer-level crystalline roughness to the AlGaIn surface.⁷⁰ As a result, lattice disorder and/or a high density of dangling bonds near step edges remained at the AlGaIn surface, leading to the generation of high-density electronic states with a continuous energy distribution. During ICP etching using the Cl_2/BCl gas mixture, active Cl-based radicals dominantly react with the AlGaIn surfaces to form volatile products, such as GaCl_3 and AlCl_3 . However, there are other possible chemical reactions. For instance, a highly volatile NCl_3 can be formed by a reaction between the Cl-based radical and N atoms, causing a preferential loss of N atoms at the AlGaIn surface.³⁸ In fact, Fang et al.⁷² reported that several kinds of deep levels originating from defect complexes related to nitrogen vacancy were increased at the GaN surface after the Cl_2 -based ICP etching. It is thus likely that ICP etching causes the monolayer-level interface rough-

ness, disorder of the chemical bonds and formation of various types of defect complexes at the AlGaIn surface, leading to poor C - V characteristics due to high-density interface states at the $\text{Al}_2\text{O}_3/\text{AlGaIn}$ interface.

4.4 V_{th} fluctuation issue in MIS AlGaIn/GaN HEMTs

Although various kinds of insulator materials have been applied to improve the performance of AlGaIn/GaN HEMTs, several problems remain unsolved. Among the most serious issues is the V_{th} fluctuation. Several papers reported that different gate bias conditions cause the V_{th} shifts in MIS HEMTs.^{13–15} Fixed charges in insulator films,^{28,50} border traps⁵¹ and interface states at the insulators/AlGaIn interfaces are involved in the V_{th} shift mechanism. As shown in Fig. 5(b), a higher interface state density leads to a shallower V_{th} . In addition, the charging state of the interface traps varies with the gate bias (E_{F} position), as shown in Fig. 7, and the deeper states with long time constants for electron emission contribute to a slow V_{th} fluctuation.¹⁴ Lu et al.¹⁵ and Johnson et al.¹⁴ reported that the higher positive gate biasing of the MIS HEMTs induces larger V_{th} shift toward the forward bias direction. This is mainly related to the change in the density of ionized acceptor-type states, as shown in Fig. 7. Ćapajna and Kuzmik¹³ also pointed out the effect of interface states on the V_{th} shift in MIS HEMTs. To realize normally-off operation, a combination of a recessed and an insulated gate structure is often implemented in AlGaIn/GaN HEMTs. However, dry etching process step for the formation of the recessed structure introduces some kinds of surface defects, resulting in high densities of electronic states at insulator/(Al)GaIn interfaces, as shown in Fig. 11 and as reported in Refs. 47 and 70.

Yang et al.⁴⁴ demonstrated that surface nitridation of GaN/AlGaIn/GaN structure using remote N_2 plasma is effective in improving a sub-threshold gate control and V_{th} stability of the Al_2O_3 -gate HEMT. Hori et al.⁷³ reported that N_2O radical treatment can decrease interface states at the $\text{Al}_2\text{O}_3/\text{AlGaIn}$ interface, resulting in the improved stability of V_{th} even after applying an off-stress gate bias. Van Hove et al.³ utilized in-situ SiN_x as an interfacial control layer, and reported improved operation stability with a small V_{th} fluctuation in the $\text{SiN}_x/\text{Al}_2\text{O}_3$ gated AlGaIn/GaN HEMT. On the basis of a systematic characterization of interface states, further investigation is absolutely necessary to control electronic states at insulator/(Al)GaIn interfaces for improved stability of AlGaIn/GaN MIS HEMTs.

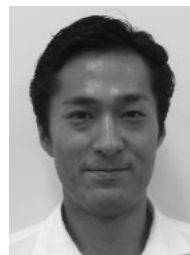
5. Conclusions

It is inevitable to make use of insulator films for insulated-gate and surface-passivation structures in the GaN-based power switching transistors. In this regard, we have reviewed important reports on the characterization of interface properties of GaN MIS structures and operation characteristics of MIS AlGaIn/GaN HEMTs. SiO_2 is an attractive insulator material due to its favorable dielectric properties such as large bandgap and high chemical stability. A high-temperature deposition and/or a high-temperature annealing process can effectively reduce state density at the SiO_2/GaN interface. SiN_x is also an important passivation material for GaN-based transistors. In-situ deposition of SiN_x during the MOCVD growth process can improve the operation stability

of HEMTs. Meanwhile, $\text{Al}_2\text{O}_3/\text{GaN}$ structures have relatively high band offsets and low interface state densities making them promising for MIS HEMT technologies. However, special attention should be given to subsequent process temperatures because a high temperature process can lead to microcrystallization of some regions in the Al_2O_3 layer. We presented a calculation method of C - V characteristics for the HEMT MIS structures for evaluating the electronic state properties at the insulator/AlGaIn interfaces. A comparison between experimental and simulation results showed that only a limited energy region of interface states is detectable using the standard C - V analysis at RT. To evaluate near-midgap electronic states at insulator/AlGaIn interfaces at RT, we have developed photo-assisted C - V method where a monochromatic light with energy less than the bandgap of AlGaIn is used. For the first time, we have estimated the state density distributions of the $\text{Al}_2\text{O}_3/\text{AlGaIn}$ interfaces using the combination of the numerical fitting of C - V curves and the photo-assisted C - V method. Further investigation on interface states is absolutely necessary for improved operation stability of AlGaIn/GaN MIS HEMTs.

- 1) K. Shinohara, D. C. Regan, Y. Tang, A. L. Corrión, D. F. Brown, J. C. Wong, J. F. Robinson, H. H. Fung, A. Schmitz, T. C. Oh, S. J. Kim, P. S. Chen, R. G. Nagele, A. D. Margomenos, and M. Micovic, *IEEE Trans. Electron Devices* **60**, 2982 (2013).
- 2) M. Ishida, T. Ueda, T. Tanaka, and D. Ueda, *IEEE Trans. Electron Devices* **60**, 3053 (2013).
- 3) M. Van Hove, X. Kang, S. Stoffels, D. Wellekens, N. Ronchi, R. Venegas, K. Geens, and S. Decoutere, *IEEE Trans. Electron Devices* **60**, 3071 (2013).
- 4) T. Kikkawa, T. Hosoda, S. Akiyama, Y. Kotani, T. Wakabayashi, T. Ogino, K. Imanishi, A. Mochizuki, K. Itabashi, K. Shono, Y. Asai, K. Joshin, T. Ohki, M. Kanamura, M. Nishimori, T. Imada, J. Kotani, A. Yamada, N. Nakamura, T. Hirose, and K. Watanabe, *Proc. 1st IEEE Workshop Wide Bandgap Power Devices and Application (WiPDA-2013)*, 2013, p. 11.
- 5) B. Hughes, R. Chu, J. Lazar, S. Hulsey, A. Carrido, D. Zehnder, M. Musni, and K. Boutros, *Proc. 1st IEEE Workshop Wide Bandgap Power Devices and Application (WiPDA-2013)*, 2013, p. 76.
- 6) Y.-F. Wu, J. Gritters, L. Shen, R. P. Smith, J. McKay, and R. Birkhahn, *Proc. 1st IEEE Workshop Wide Bandgap Power Devices and Application (WiPDA-2013)*, 2013, p. 6.
- 7) N. Herbecq, I. Roch-Jeune, N. Rolland, D. Visalli, J. Derluyn, S. Degroote, M. Germain, and F. Medjdoub, *Appl. Phys. Express* **7**, 034103 (2014).
- 8) Y. Yue, Y. Hao, J. Zhang, J. Ni, W. Mao, Q. Feng, and L. Liu, *IEEE Electron Device Lett.* **29**, 838 (2008).
- 9) J. Shi and L. F. Eastman, *IEEE Electron Device Lett.* **32**, 312 (2011).
- 10) C. Mizue, Y. Hori, M. Miczek, and T. Hashizume, *Jpn. J. Appl. Phys.* **50**, 021001 (2011).
- 11) Z. H. Liu, G. I. Ng, S. Arulkumaran, Y. K. T. Maung, K. L. Teo, S. C. Foo, and V. Sahnuganathan, *Appl. Phys. Lett.* **95**, 223501 (2009).
- 12) S. L. Selvaraj and T. Egawa, *J. Electrochem. Soc.* **156**, H690 (2009).
- 13) M. Ćapajna, M. Jurković, L. Válik, Š. Haščík, D. Gregušová, F. Brunner, E.-M. Cho, and J. Kuzmik, *Appl. Phys. Lett.* **102**, 243509 (2013).
- 14) D. W. Johnson, R. T. P. Lee, R. J. W. Hill, M. H. Wong, G. Bersuker, E. L. Piner, P. D. Kirsch, and H. R. Harris, *IEEE Trans. Electron Devices* **60**, 3197 (2013).
- 15) Y. Lu, S. Yang, Q. Jiang, Z. Tang, B. Li, and K. J. Chen, *Phys. Status Solidi C* **10**, 1397 (2013).
- 16) J. Robertson and B. Falabretti, *J. Appl. Phys.* **100**, 014111 (2006).
- 17) Y. Hori, C. Mizue, and T. Hashizume, *Jpn. J. Appl. Phys.* **49**, 080201 (2010).
- 18) S. Miyazaki, *J. Vac. Sci. Technol. B* **19**, 2212 (2001).
- 19) M. L. Huang, Y. C. Chang, Y. H. Chang, T. D. Lin, J. Kwo, and M. Hong, *Appl. Phys. Lett.* **94**, 052106 (2009).
- 20) T. Hashizume, S. Ootomo, T. Inagaki, and H. Hasegawa, *J. Vac. Sci. Technol. B* **21**, 1828 (2003).
- 21) T. E. Cook, Jr., C. C. Fulton, W. J. Mccouch, R. F. Davis, G. Lucovsky, and R. J. Nemanich, *J. Appl. Phys.* **94**, 3949 (2003).
- 22) C.-T. Lee, H.-Y. Lee, and H.-W. Chen, *IEEE Electron Device Lett.* **24**, 54 (2003).

- 23) T. S. Lay, Y. Y. Liao, W. H. Hung, M. Hong, J. Kwo, and J. P. Mannaerts, *J. Cryst. Growth* **278**, 624 (2005).
- 24) T. E. Cook, Jr., C. C. Fulton, W. J. Mecoouch, R. F. Davis, G. Lucovsky, and R. J. Nemanich, *J. Appl. Phys.* **94**, 7155 (2003).
- 25) F. Tian and E. F. Chor, *Thin Solid Films* **518**, e121 (2010).
- 26) B. Gaffey, L. J. Guido, X. W. Wang, and T. P. Ma, *IEEE Trans. Electron Devices* **48**, 458 (2001).
- 27) T. E. Cook, Jr., C. C. Fulton, W. J. Mecoouch, K. M. Tracy, R. F. Davis, E. H. Hurt, G. Lucovsky, and R. J. Nemanich, *J. Appl. Phys.* **93**, 3995 (2003).
- 28) M. Esposto, S. Krishnamoorthy, D. N. Nath, S. Bajaj, T.-H. Hung, and S. Rajan, *Appl. Phys. Lett.* **99**, 133503 (2011).
- 29) K. Matocha, R. J. Gutmann, and T. P. Chow, *IEEE Trans. Electron Devices* **50**, 1200 (2003).
- 30) E. Kim, N. Soejima, Y. Watanabe, M. Ishiko, and T. Kachi, *Jpn. J. Appl. Phys.* **49**, 04DF08 (2010).
- 31) M. Kanechika, M. Sugimoto, N. Soejima, H. Ueda, O. Ishiguro, M. Kodama, E. Hayashi, K. Iyoh, T. Uesugi, and T. Kachi, *Jpn. J. Appl. Phys.* **46**, L503 (2007).
- 32) Y. Niiyama, T. Shinagawa, S. Ootomo, H. Kambayashi, T. Nomura, and S. Yoshida, *Phys. Status Solidi A* **204**, 2032 (2007).
- 33) W. Huang, T. Khan, and T. P. Chow, *IEEE Electron Device Lett.* **27**, 796 (2006).
- 34) H. Kambayashi, Y. Satoh, S. Ootomo, T. Kokawa, T. Nomura, S. Kato, and T. P. Chow, *Solid-State Electron.* **54**, 660 (2010).
- 35) K. Yamaji, M. Noborio, J. Suda, and T. Kimoto, *Jpn. J. Appl. Phys.* **47**, 7784 (2008).
- 36) H. Kambayashi, T. Nomura, H. Ueda, K. Harada, Y. Morozumi, K. Hasebe, A. Teramoto, S. Sugawa, and T. Ohmi, *Jpn. J. Appl. Phys.* **52**, 04CF09 (2013).
- 37) R. Nakasaki, T. Hashizume, and H. Hasegawa, *Physica E* **7**, 953 (2000).
- 38) T. Hashizume and H. Hasegawa, *Appl. Surf. Sci.* **234**, 387 (2004).
- 39) B. M. Green, K. K. Chu, E. M. Chumbes, J. A. Smart, J. R. Shealy, and L. F. Eastman, *IEEE Electron Device Lett.* **21**, 268 (2000).
- 40) J. Derluyn, S. Boeykens, K. Cheng, R. Vandersmissen, J. Das, W. Ruythooren, S. Degroote, M. R. Leys, M. Germain, and G. Borghs, *J. Appl. Phys.* **98**, 054501 (2005).
- 41) E. Ogawa, T. Hashizume, S. Nakazawa, T. Ueda, and T. Tanaka, *Jpn. J. Appl. Phys.* **46**, L590 (2007).
- 42) T. Takizawa, S. Nakazawa, and T. Ueda, *J. Electron. Mater.* **37**, 628 (2008).
- 43) M. Kanamura, T. Ohki, T. Kikkawa, K. Imanishi, T. Imada, A. Yamada, and N. Hara, *IEEE Electron Device Lett.* **31**, 189 (2010).
- 44) S. Yang, Z. Tang, K.-Y. Wong, Y.-S. Lin, C. Liu, Y. Lu, S. Huang, and K. J. Chen, *IEEE Electron Device Lett.* **34**, 1497 (2013).
- 45) R. Chu, A. Corrión, M. Chen, R. Li, D. Wong, D. Zehnder, B. Hughes, and K. Boutros, *IEEE Electron Device Lett.* **32**, 632 (2011).
- 46) K.-Y. Park, H.-I. Cho, J.-H. Lee, S.-B. Bae, C.-M. Jeon, J.-L. Lee, D.-Y. Kim, C.-S. Lee, and J.-H. Lee, *Phys. Status Solidi C* **0**, 2351 (2003).
- 47) S. Kim, Y. Hori, W.-C. Ma, D. Kikuta, T. Narita, H. Iguchi, T. Uesugi, T. Kachi, and T. Hashizume, *Jpn. J. Appl. Phys.* **51**, 060201 (2012).
- 48) S. Toyoda, T. Shinohara, H. Kumigashira, M. Oshima, and Y. Kato, *Appl. Phys. Lett.* **101**, 231607 (2012).
- 49) D. Kikuta, T. Narita, K. Kutsuki, T. Uesugi, and T. Kachi, *Jpn. J. Appl. Phys.* **52**, 08JN19 (2013).
- 50) J. Son, V. Chobpattana, B. M. McSkimming, and S. Stemmer, *Appl. Phys. Lett.* **101**, 102905 (2012).
- 51) M. Choi, J. L. Lyons, A. Janotti, and C. G. Van de Walle, *Phys. Status Solidi B* **250**, 787 (2013).
- 52) D. Deen, D. Storm, D. Meyer, D. S. Katzer, R. Bass, S. Binari, and T. Gougousi, *Phys. Status Solidi C* **8**, 2420 (2011).
- 53) T. Kikkawa, K. Makiyama, T. Ohki, M. Kanamura, K. Imanishi, N. Hara, and K. Joshin, *Phys. Status Solidi A* **206**, 1135 (2009).
- 54) S. Yang, S. Huang, M. Schnee, Q.-T. Zhao, J. Schubert, and K. J. Chen, *IEEE Trans. Electron Devices* **60**, 3040 (2013).
- 55) M. Hatano, Y. Taniguchi, S. Kodama, H. Tokuda, and M. Kuzuhara, *Appl. Phys. Express* **7**, 044101 (2014).
- 56) Y. Hayashi, S. Kishimoto, and T. Mizutani, *Solid-State Electron.* **54**, 1451 (2010).
- 57) R. Stoklas, D. Gregušová, K. Hušeková, J. Marek, and P. Kordoš, *Semicond. Sci. Technol.* **29**, 045003 (2014).
- 58) M. Fagerlind, F. Allerstam, E. Ö. Sveinbjörnsson, N. Rorsman, A. Kakanakova-Georgieva, A. Lundskog, U. Forsberg, and E. Janzén, *J. Appl. Phys.* **108**, 014508 (2010).
- 59) M. Ćapajna and J. Kuzmík, *Appl. Phys. Lett.* **100**, 113509 (2012).
- 60) M. Miczek, C. Mizue, T. Hashizume, and B. Adamowicz, *J. Appl. Phys.* **103**, 104510 (2008).
- 61) H. Luth, *Surfaces and Interfaces of Solids* (Springer, Heidelberg, 1993) 2nd ed., p. 381.
- 62) W. Mönch, *Appl. Surf. Sci.* **117–118**, 380 (1997).
- 63) R. Stoklas, D. Gregušová, J. Novák, A. Vescan, and P. Kordoš, *Appl. Phys. Lett.* **93**, 124103 (2008).
- 64) J. J. Freedsmann, T. Kubo, and T. Egawa, *Appl. Phys. Lett.* **99**, 033504 (2011).
- 65) H.-A. Shih, M. Kudo, and T. Suzuki, *Appl. Phys. Lett.* **101**, 043501 (2012).
- 66) R. Yeluri, B. L. Swenson, and U. K. Mishra, *J. Appl. Phys.* **111**, 043718 (2012).
- 67) M. Fagerlind and N. Rorsman, *J. Appl. Phys.* **112**, 014511 (2012).
- 68) M. Matys, B. Adamowicz, and T. Hashizume, *Appl. Phys. Lett.* **101**, 231608 (2012).
- 69) M. Matys, B. Adamowicz, Y. Hori, and T. Hashizume, *Appl. Phys. Lett.* **103**, 021603 (2013).
- 70) Z. Yatabe, Y. Hori, S. Kim, and T. Hashizume, *Appl. Phys. Express* **6**, 016502 (2013).
- 71) S. Ozaki, T. Ohki, M. Kanamura, N. Okamoto, and T. Kikkawa, *Jpn. J. Appl. Phys.* **52**, 11NG04 (2013).
- 72) Z.-Q. Fang, D. C. Look, X.-L. Wang, J. Han, F. A. Khan, and I. Adesida, *Appl. Phys. Lett.* **82**, 1562 (2003).
- 73) Y. Hori, Z. Yatabe, and T. Hashizume, *J. Appl. Phys.* **114**, 244503 (2013).



Zenji Yatabe received his Ph. D. degree in Biochemistry and Biotechnology from the Tokyo University of Agriculture and Technology (TUAT), Tokyo, Japan, in 2008. In 2011, he joined the Research Center for Integrated Quantum Electronics (RCIQE) of the Hokkaido University as a Post-doctoral fellow. His research interests include characterization and control of surfaces and interfaces of GaN and related materials.



Yujin Hori received the Ph. D. degree in Information Science and Technology from Hokkaido University, Sapporo, Japan, in 2014. His research interests included surface-interface characterization of GaN and related materials. In 2014, he joined Furukawa Electric Corporation, Yokohama, Japan.



Wan-Cheng Ma received the MS degree in Information Science and Technology from Hokkaido University, Sapporo, Japan, in 2014. His research interests include surface-interface characterization of GaN and related materials. In 2014, he joined Denso Corporation, Kariya, Japan.



Joel T. Asubar received his Ph. D. degree from the Nagaoka University of Technology, Niigata, Japan, working on molecular beam epitaxial growth of ferromagnetic semiconductors. In 2010, he joined the Research Center for Integrated Quantum Electronics (RCIQE) of the Hokkaido University as a Post-doctoral fellow. His research interests include growth of semiconductor heterojunctions, fabrication, characterization and reliability studies of GaN-based transistors.



Masamichi Akazawa received his B.S. and Ph. D. degrees in Electrical Engineering from Hokkaido University in 1988 and 1994, respectively. He is currently an Associate Professor at Research Center of Integrated Quantum Electronics, Hokkaido University, Japan. His recent work has been on surface/interface characterization of III–V compound semiconductors. His present research interests include surface/interface characterization and device application of III–nitride alloys.



Taketomo Sato received his Ph. D. degree from Hokkaido University in 2001. Since 2004, he has been an Associate Professor of Research Center for Integrated Quantum Electronics (RCIQE), Hokkaido University. His research interests include photo-electrochemical process for III-V compound semiconductors. Currently, his major activity has expanded into low-damage etching and nanostructure fabrication of GaN and related materials.



Tamotsu Hashizume received his Ph. D. degree from Hokkaido University in 1991. Since 2004, he has been a Professor of Research Center for Integrated Quantum Electronics (RCIQE), Hokkaido University. He is currently the director of RCIQE. His research interests include surface passivation and device processing technologies for III-V compound semiconductors. Presently, his major activity has expanded into characterization and control of surfaces and interfaces of GaN and related materials

and their application to GaN-based electron devices. He has authored or co-authored over 160 papers in scientific and technical journals.